PERGAMON

International Journal of Heat and Mass Transfer 45 (2002) 2107–2117

International Journal of HEAT and MASS TRANSFER

www.elsevier.com/locate/ijhmt

Experimental study on laminar flow forced-convection in a channel with upper V-corrugated plate heated by radiation

Ahmed Hamza H. Ali [a,*], Yutaka Hanaoka [b]

[a] *Mechanical Engineering Department, Faculty of Engineering, Assiut University, Assiut 71516, Egypt*
[b] *Department of Mechanical Systems Engineering, Muroran Institute of Technology, Muroran 050-8585, Japan*

Received 31 December 2000; received in revised form 10 August 2001

Abstract

Experimental study of the effects of the operating parameters on laminar flow forced-convection heat transfer for air flowing in a channel having a V-corrugated upper plate heated by radiation heat flux while the other walls are thermally insulated has been carried out. The parameters studied and their ranges were as follows: flow Reynolds number (Re) ranging from 750 to 2050, incident radiation fluxes (q_{inc}) of 400, 700, and 1000 W/m^2, inlet air bulk temperatures ($T_{b,in}$) ranging from 12.4 to 59.4 °C and tilting angles of the channel (β) of 0°, 15°, 30°, 45°, and 60°. The results show that, the effect of Re on local Nusselt number (Nu_x) are clear and more significant at the channel entrance region. While, changing β from 0° to 60° leads to an increase in Nu_x by a ratio ranging from 33% to 67.3% depending on Re values and other operating parameters. Increasing the q_{inc} values by 175% and 250% leads to an increase in Nu_x values by 26% and 50%, respectively. In addition, the results indicate that there are significant increases in Nu_x in the channel entrance region due to the increase in inlet air bulk temperature and this influence diminishes downstream.

1. Introduction

Characteristics of laminar flow forced-convection heat transfer for air flowing in a channel having a V-corrugated upper plate heated by radiation heat flux and thermally insulated flat sidewalls and bottom is an important subject for air heater solar collectors applications. Conventional heat exchangers are known to accomplish a fluid-to-fluid heat exchange with radiation as a negligible factor, while solar air heater collectors, which are special types of heat exchangers, use solar radiation to heat the air (working fluid). However, because of the low thermal and hydrodynamic properties of the air, solar air collectors have the disadvantage of low convective heat transfer coefficient compared with those that use liquids as working fluids. The use of a V-corrugated plate as an absorber in a solar air collector improves its thermal performance for two reasons. First, corrugations enhance the convective heat transfer coefficient (h) and at the same time the effective convective heat transfer area (A) increases, resulting in a collective increase of the convective conductance (hA). The second reason is that, the V-corrugated plate absorber provides an apparent absorptivity to the incident radiation flux of almost unity even when painted with commercial black paint, as indicated by Sparrow and Lin [1]. Published data for the convective heat transfer coefficient in (inverted V shapes) triangular channels were reported for both constant heat flux and isothermal conditions cases in [2–4]. Piao et al. [5] studied the forced convection in cross-corrugated channel subjected to radiation heat flux. Sparrow and Lin [1] reported that, the maximum absorbed thermal energy in a V-groove cavity subjected to radiation heat flux takes place near the apex. Effects of convection–radiation interaction on the convective heat transfer coefficient for laminar flow in a parallel plate channel were studied analytically by Liu and

* Corresponding author.
E-mail address: ah-hamza@acc.aun.eun.eg (A.H.H. Ali).

0017-9310/02/$ - see front matter
PII: S0017-9310(01)00309-X

Nomenclature

A	surface area, m^2
D_h	flow hydraulic diameter at inlet of the test section, m
h	convective heat transfer coefficient, W/m^2 K
i	element number
k	thermal conductivity, W/m K
n	number of elements, dimensionless
Nu_x	local Nusselt number, dimensionless
q	heat flux, W/m^2
Q	heat transfer rate, W
Re	Reynolds number, $u_{in}D_h/v_{in}$, dimensionless
T	temperature, K or °C
u	average flow velocity in x-direction, m/s
x	axial horizontal distance measured from the V-corrugated plate inlet edge, mm

Greek symbols

α	absorptance, dimensionless
β	the unit inclination angle with the horizontal, degree
ρ	reflectance, dimensionless
τ	transmittance, dimensionless
v	kinematic viscosity, kg/m s

Subscripts

a	ambient
abs	absorbed radiation
air	flowing air
b	bulk temperature
bk	back plate
cond	conduction
conv	convection
g	glass sheet cover
i	element i
in	inlet
inc	incident radiation
out	outlet
rad	radiation
sur	surrounding surfaces to the test section
vpl	V-corrugated plate (absorber)

Sparrow [6]. Such combined effects were numerically studied for flow in an asymmetrically heated duct by Satoh and Kurosaki [7]. Based on the previous findings it can be concluded that, not only higher temperature values exist at the apex's of the V shapes as indicated in [1], in the case of triangular channel, but also high local fluid temperature zones exist due to close stagnant flow regimes around the apex's of these channels. Both of these factors decrease the net useful convected heat transfer to the flowing air. Also, based on the results of [6,7], for air flowing in laminar flow regime through a channel having one wall heated by a constant heat flux and the other walls being thermally insulated, the convective heat transfer coefficient is a function of the heat flux. In the present study, it is proposed to move the bottom plate of the triangular shapes to form a channel with a V-corrugated upper plate heated by radiation heat flux and thermally insulated flat sidewalls and bottom wall. This configuration is expected to enhance the convective heat transfer processes for solar air collectors' applications. The aim of this work is to study experimentally the effects of different operating parameters on the convective heat transfer coefficient in laminar flow regime, for the suggested channel configuration which is formed by an upper V-corrugated plate heated by radiation flux and thermally insulated flat sides and bottom. The operating factors studied are the incident radiation heat flux, Reynolds number, inlet air bulk temperature, and the tilting angle of the unit with the horizontal.

2. Experimental apparatus, instrumentations and procedure

2.1. Apparatus and measuring instrumentations

A schematic diagram of both the apparatus and flow channel configurations and dimensions are shown in Fig. 1. The apparatus consists mainly of an air-handling section, test section, radiation heat flux source and the measuring instrumentations.

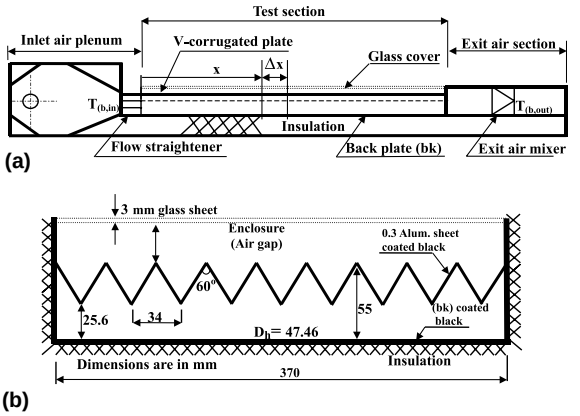

Fig. 1. Schematic drawing of the experimental apparatus (a) main sections of the apparatus, and (b) configuration and dimensions of the flow channel cross-section.

2.1.1. Air-handling sections

The air-handling sections for this apparatus include the inlet section and exit air mixing section. The inlet section incorporates an inlet air heater, an axial flow fan, orifice meter, inlet air distribution plenum and flow straightener (honeycomb). The inlet air heater was used to study the effect of the inlet air bulk temperature as an operating parameter, which was controlled by the input power to the electric heater. A variable electric resistor controls the input power to the fan motor to change the axial fan speed and consequently the air volume flow rate. The air volume flow rate was measured with a 300 mm in diameter sharp edge orifice plate. The calibration curve for this orifice is given in [8]. The velocity of the air passing through the orifice throat was determined in terms of the static pressure drop across the orifice plate, which was measured using Göttingen water manometer type F-210 having a range 0–300 mm water with an accuracy of ±0.05 mm. The air leaving the test section passed through the exit air section, which is mainly an air mixer, within which the outlet air bulk temperature (mixed mean) is measured.

2.1.2. Test section

The overall dimensions of the test section shown in Fig. 1(a) are 0.9 m in length, 0.4 m in width, and 90 mm in depth, with a back plate made from aluminum sheet of 0.5 mm in thickness and has a 3 mm colorless glass cover. The back plate and sidewalls of the test section are thermally insulated by 50 mm glass fiber (thermal conductivity about 0.038 W/m K) and are contained in an outer hardwood frame. A V-corrugated plate with apex angle of 60° placed below the glass cover forms the airflow channel below it with the back plate and the sidewalls, and at the same time an enclosure air gap is formed between its upper surface and the glass cover as shown in Fig. 1(b). The V-corrugated plate (absorber) is an aluminum sheet with net dimensions of 0.88 m in length, 0.37 m in width, and 0.3 mm in thickness. Thus, the net projected area subjected to the radiation heat flux is 0.3256 m^2. The upper surfaces of both the V-corrugated plate and the back plate were coated with a commercial black paint, with an average coating thickness of about 60 μm. The monochromatic reflectance of a coated black aluminum sheet sample was measured in the spectrum range 0.22–0.85 μm using an integration sphere attachments of a Spectrophotometer system model UV-2200 (Manufactured by Shimadzu, Japan). While in the spectrum range of 1–25 μm, the monochromatic reflectance was measured using the total diffuse reflectance attachments of a Spectrophotometer System 2000 FT-IR (Manufactured by Perkin–Elmer, England). The results of both measurements were used to estimate the spectral absorptance values over the whole range as presented in Fig. 2. As seen from the figure, the average value of the monochromatic absorptance in the wavelength range of 0.3–25 μm is about 0.94. The normal monochromatic transmittance and reflectance of the colorless glass cover used in this work were reported by the manufacture and is presented in Fig. 2. The reported average normal transmittance of this glass in the spectrum range 0.3–3 μm is 0.855.

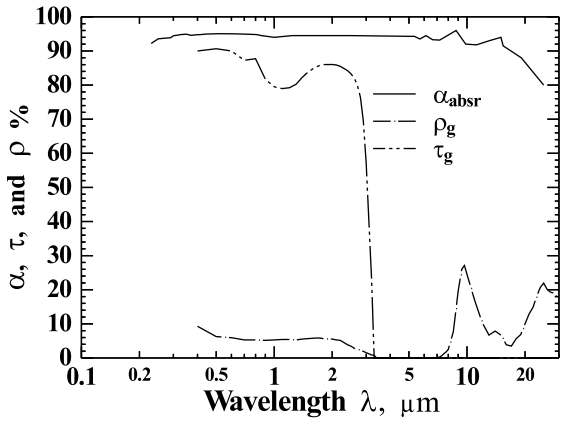

Fig. 2. Measured total spectral absorptance of the coated black V-corrugated aluminum plate, and both the spectral reflectance and transmittance of 3 mm thickness glass cover.

2.1.3. Radiation heat flux source

The top plane of the test section (glass sheet) is uniformly heated by an incident radiation heat flux. The radiation heat source is an assembly of 10 tungsten lamps whose maximum filament temperature is 2850 K at the full load condition. The lamps are fixed to a frame having the same area as that of the test section, and is placed parallel to it at 1 m above the glass cover. This set of lamps is capable of delivering radiation heat fluxes at the plane of the glass cover, in wavelength ranging from 0.25 to 3 μm and intensities ranges between a minimum and maximum values of 420–1140 W/m^2, respectively. During the experiments, a chosen value of the incident radiation flux was adjusted by the input power to the lamps, which is controlled by Thyristor power control. The incident radiation flux was measured at the surface of the glass cover by using EKO pyranometer, type Ms-42, having sensitivity of 7 mV/kW m^{-2} with an error of 0.1% due to temperature variation. The pyranometer glass dome spectral transmittance for a wavelengths up to 3 μm, (pyranometer measuring range) is shown in Fig. 3. The average value of the incident radiation flux on the test section top plane was determined as follows. The plane of the glass cover was divided into 18 sectors, and the measurement of the incident radiation heat flux was performed at each sector separately corresponding to each input power to the lamps. The deviation of individual sectors measured values from that of the overall average values ranged from −5.3% to 4.3%. This error

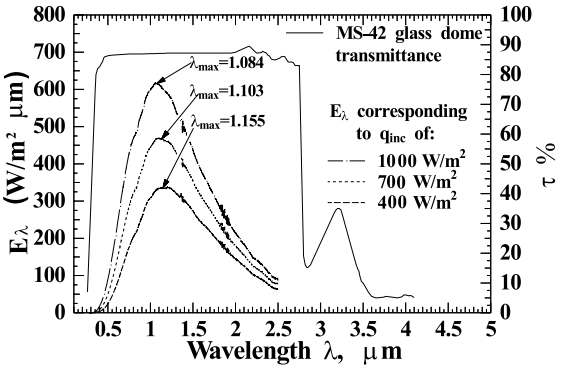

Fig. 3. Measured spectral emissive power of a Ref-lamp and the spectral transmittance of Ms-42 pyranometer glass dome.

range is within the allowable deviation of the indoor tests for solar collector performance standards [9,10], which indicate that deviations up to ±10% are acceptable. The spectral radiation power distributions for one-lamp corresponding to three different incident radiation fluxes (400, 700 and 1000 W/m^2) were measured using spectral pyranometer type MSR-7000 (Manufactured by Optic Research, Japan). The measured data at different values of incident radiation fluxes are presented in Fig. 3. From Figs. 2 and 3 it can be seen that, the range of the Ms-42 pyranometer glass dome (measuring range) and that of the glass cover transmittance coincide up to about 3 μm. Also, Fig. 3 shows that the lamp(s) spectral radiation power vanishes after a wavelength of 2.5 μm. This means that, the lamps incident radiation heat flux is completely within the measuring range of the Ms-42 pyranometer. Moreover, the transmitted radiation flux through the glass cover to the V-corrugated plate is the only measured and recorded value by Ms-42 pyranometer.

2.1.4. Temperature measurements

A 60 channels acquisition system, which is a Remote scanner DE 1000 data acquisition system that has a resolution of ±0.1 °C, was used for the temperature measurements and recording. All temperatures were measured by using Type T (copper/constantan) thermocouple. Two sizes of thermocouple wires were used. The first size is a 0.1 mm in diameter, which has the junction in contact with the component for which the temperature is to be measured. The second size is an extension thermocouple wire (Type T) of 0.32 mm diameter used to connect the 0.1 mm wire diameter thermocouple (some distance away from the contact point) to the temperature recorder. The thermocouples were used to measure the temperature distributions at the following locations: 10 points along x-axis of the V-corrugated plate (the flow direction), 4 points at two axial sections of the V-corrugated plate, 19 points at two x-axial locations uniformly distributed on the middle V walls, 6 points in the glass cover along x-axis, 16 points distributed over the back plate, sidewalls and outer sides of the housing frame. The thermocouples in the width direction were used to check the conduction effect in the lateral direction. In addition, temperature measurements were carried out at the following locations (one point each): inlet air bulk temperature, ambient air, mean air bulk at the exit section, lamps frame holder, and the upper assembly frame. The error in the thermocouples reading reported by the manufacture based on Japanese Industrial standard (JIS) was about ±0.5 °C.

2.2. Experimental procedures

The operating parameters studied and their ranges were as follows: air mass flow rate corresponding to *Re* values ranging from 750 to 2050, incident radiation fluxes were 400, 700, 1000 W/m^2, inlet air bulk temperature ranged from 12.4 to 59.4 °C and tilting angles of the channel with the horizontal were 0°, 15°, 30°, 45°, and 60°, respectively. The stabilization of temperature readings to ±0.1 °C in all thermocouple sensors was considered an indication of reaching steady-state condition. For almost all the experimental runs, this condition was established and reached within 5–6 h depending on the *Re* value inside the test section. At this time, the average of the temperature values read and recorded by the data acquisition system during the last 5 min is considered a good representation of the temperature at such location. In addition, the manometer reading for the pressure difference across the orifice was taken at that time. To study the influence of one of the operating parameters, the previous procedures were repeated at a different value of this parameter with other controlled operating parameters kept constant. The only uncontrolled parameter was the ambient air temperature during these experiments.

2.3. Data reduction and determination of the convection heat transfer coefficient

To fulfill the objectives of the present study, the variation of the local convective heat transfer coefficient (h), presented in Nu_x form defined by Eq. (1), under different operating parameters was determined and analyzed. Therefore, the measured data were used along with the values of other controlled operating parameters to determine the variation of (h) with the axial distance under different conditions. The model used to determine the local convective heat transfer coefficient (h) has been formulated by performing an energy balance on each of the test section components based on the following assumptions:

1. One-dimensional temperature variation along the flow direction. This assumption has been verified by

the reading of three thermocouples across the V-corrugated plate perpendicular to the flow direction at two different axial positions and by the reading of the 19-thermocouple points on the middle V-walls at two x-axis locations. The differences between thermocouple readings in the transverse direction at all locations were ±0.8 °C of the average value.

2. Uniform incident radiation flux over the glass cover, and consequently over the V-corrugated plate as indicated by the incident radiation flux measurements.
3. Uniform thermal radiation transfer between all channel surfaces, which are to be estimated based on the surfaces average temperatures.
4. The natural convection within the air gap is estimated based on the average values of the convection heat transfer coefficient within the enclosure and the average surfaces temperatures.
5. Linear variation of the flowing air bulk temperature between the test section inlet and outlet.

2.3.1. Energy balance on different components of the test section

The test section is divided along the flow direction into n elements of equal width Δx as shown in Fig. 1(a). The local Nusselt number Nu_x for an element i at an axial position x is given by

$$Nu_x = h_{(\mathrm{vpl,air})x}\, D_\mathrm{h}/k_{\mathrm{air},i}, \tag{1}$$

where

$$h_{(\mathrm{vpl,air}),x} = \frac{q_{\mathrm{conv(vpl,air)}i}}{(T_{\mathrm{vpl},i} - T_{\mathrm{b},i})} \quad (\mathrm{W/m^2\ K}),$$

where $q_{\mathrm{conv(vpl,air)}i}$ is the local convective heat transfer flux from V-corrugated plate element i to the air-stream element, $T_{\mathrm{vpl},i}$ is the temperature of V-corrugated plate element i (measured quantity), $T_{\mathrm{b},i}$ is the air-stream bulk temperature of the element i and it is obtained by interpolation from the measured values of the inlet and outlet air bulk temperatures ($T_{\mathrm{b,in}}$ and $T_{\mathrm{b,out}}$) assuming a linear axial distribution. The value of $q_{\mathrm{conv(vpl,air)}i}$ can be obtained by applying the energy balance equations at the element i on each component of the test section (glass cover, V-corrugated plate and back plate) as follows:

(a) *Glass cover*

$$A_{\mathrm{g},i}\alpha_\mathrm{g} q_\mathrm{inc} + Q_{\mathrm{cond,g},i} + Q_{\mathrm{conv(vpl,g)}}/n + Q_{\mathrm{rad(vpl,g)}}/n = A_{\mathrm{g},i} q_{\mathrm{conv(g,a)}i} + Q_{\mathrm{rad(g,sur)}}/n \quad (\mathrm{W}), \tag{2}$$

where $Q_{\mathrm{cond,g},i}$ is the axial heat conduction into the node i.

$Q_{\mathrm{conv(vpl,g)}}$ is the natural convection heat transfer from the V-corrugated plate to the glass cover which is given by

$$Q_{\mathrm{conv(vpl,g)}} = A_\mathrm{g} h_{\mathrm{g,vpl}} (T_\mathrm{vpl} - T_\mathrm{g}) \quad (\mathrm{W}), \tag{3}$$

where A_g is the glass cover surface area, T_g and T_vpl are the estimated average temperatures of the glass cover and V-corrugated plates, respectively and $h_{\mathrm{g,vpl}}$ is the free convective heat transfer coefficient between them, which was calculated using the formula given by El-Sherbiney et al. [11]. $Q_{\mathrm{rad(vpl,g)}}$ is the net thermal radiation heat transfer rate from the V-corrugated plate to the glass cover. $q_{\mathrm{conv(g,a)}i}$ is the natural convective heat transfer flux out from the glass cover element i to the ambient air, in which the natural convective heat transfer coefficient ($h_{\mathrm{conv(g,a)}i}$) was calculated using the formula given by Fujii and Imura [12]. $Q_{\mathrm{rad(g,sur)}}$ is the thermal radiation heat transfer rate out from the glass cover to the surrounding. α_g is the glass cover absorptivity in the wavelength range 0.3–3 μm, which is estimated from Fig. 2 to be $\alpha_\mathrm{g} = 0.095$.

(b) *V-corrugated plate*

$$\tau_\mathrm{g}\alpha_{\mathrm{(vpl)a}} A_{\mathrm{vpl},i} q_\mathrm{inc} + Q_{\mathrm{cond,vpl},i} = Q_{\mathrm{conv(vpl,g)}}/n + Q_{\mathrm{rad(g,vpl)}}/n + A_{\mathrm{vpl},i} q_{\mathrm{conv(vpl,air)}i} + Q_{\mathrm{rad(bk,vpl)}}/n \quad (\mathrm{W}), \tag{4}$$

where $\alpha_{\mathrm{(vpl)a}}$ is the upper surface of the V-corrugated plate apparent absorptivity and τ_g is the glass cover transmittance. The average measured values of α_vpl (α_vpl is the absorptivity of a flat aluminum sheet sample coated with black paint) and τ_g in the wavelength range 0.3–3 μm as shown in Fig. 2 are $\alpha_\mathrm{vpl} = 0.94$ and $\tau_\mathrm{g} = 0.855$. However, based on the results of [1] for V-groove diffuse surface absorber with considering the multiple reflections and absorption of the beam flux, thus the apparent V-groove absorptivity value $\alpha_{\mathrm{(vpl)a}}$ is 1.0.

(c) *Back plate*

$$Q_{\mathrm{rad(vpl,bk)}}/n = Q_{\mathrm{cond(bk)}i} + A_{\mathrm{bk},i} q_{\mathrm{conv(bk,air)}i} \quad (\mathrm{W}), \tag{5}$$

where $Q_{\mathrm{cond(bk)}i}$ is the conduction heat transfer out from the backside of back plate element i to the outer surface of the housing through the thermal insulation. $Q_{\mathrm{rad(vpl,bk)}}$ is the net thermal radiation heat transfer input to the back plate from the V-corrugated plate.

2.3.2. Procedure for determination of the convection heat transfer coefficient

From the energy balance Eqs. (2), (4), and (5), the values of $q_{\mathrm{conv(vpl,air)}i}$, can be estimated at different axial positions (elements) along the flow direction at specified operating conditions. The obtained values are substituted in Eq. (1). To determine the variation of the convection heat transfer coefficient within the axial direction for a certain operating parameter, this procedure is repeated. The uncertainty in the estimated

quantities of this work was calculated based on equations for computing the probable errors or uncertainties as given by Holman [13] and the formula for computing overall errors as given by Doblen [14]. Based on these formulas and from the measured values of all operating parameters, the estimated uncertainty were as follows: for mass flow rate $\leqslant 7.3\%$, for the incident radiation flux $\leqslant 5.3\%$, for net absorbed radiation in the V-corrugated plate was $\leqslant 7.8\%$. However, this leads to the estimated error in the determined local Nusselt number is $\pm 11.4\%$.

3. Results and discussion

The results of the present work cover the influence of different controlled operating parameters on the convective heat transfer coefficient in terms of local Nusselt number (Nu_x). These parameters are the air mass flow rate in terms of Reynolds number values (Re), incident radiation heat flux (q_{inc}), angle of inclination of the test unit with the horizontal (β), and the inlet air bulk temperature ($T_{b,in}$).

3.1. Temperature distributions

Effects of the flow Reynolds number values on the V-corrugated plate axial temperature distributions for the case of $\beta = 0°$ at different values of incident radiation fluxes are shown in Fig. 4. The effect of Re on such distribution for the cases with $\beta = 15°, 45°$ and $60°$ are shown in Fig. 5 at q_{inc} of 700 W/m^2. It can be seen from Figs. 4 and 5 that for the same incident radiation flux the highest V-corrugated plate temperature distribution in the x-direction were recorded in case of $\beta = 0°$ at low Re values. On the other hand, the figures show that, the effect of Re on T_{vpl} decreases as β increases and almost

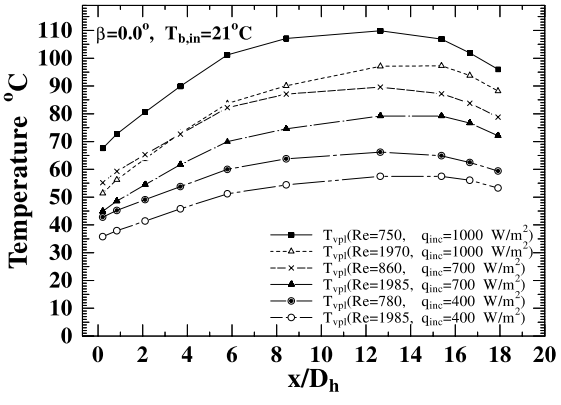

Fig. 4. Effect of Reynolds number on the V-corrugated plate axial temperature distributions for $\beta = 0°$ at different incident radiation fluxes.

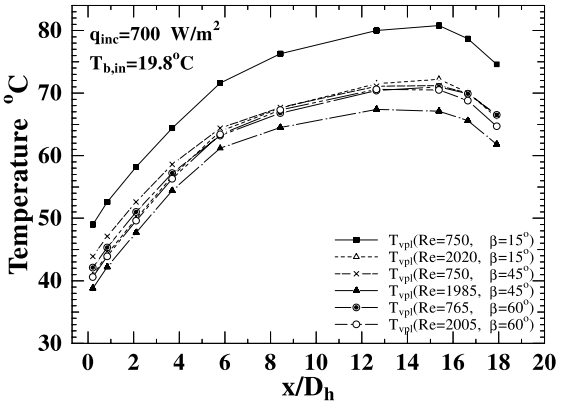

Fig. 5. Effect of Reynolds number on the V-corrugated plate temperature distributions for $\beta > 0°$ at $q_{inc} = 700$ W/m^2.

vanishes when β reaches 60° as shown in Fig. 5. Of course, higher values of T_{vpl} are followed by higher values of $T_{b,out}$ as it is expected. The values of $T_{b,out}$ corresponding to T_{vpl} distributions presented in Fig. 4 for q_{inc} value of 700 W/m^2, were 42.8 and 36.5 °C for Re values of 860 and 1985, respectively. Comparison of the effect of Re for $\beta > 0°$ on the V-corrugated plate temperature distributions values that are shown in Fig. 5, with the case of $\beta = 0°$ that are shown in Fig. 4, shows that at q_{inc} of 700 W/m^2 as β was increased the values of T_{vpl} decreased, consequently, $T_{b,out}$ values also decreases. This can be explained as follows: as β increases the effect of the buoyancy force component in the flow direction ($g \sin \beta$) inside the V-shaped of the channel increases particularly at high q_{inc} values. This resulted in accelerating the fluid in the thermal boundary layer, consequently, increasing the convection heat transfer rate released from the V-corrugated plate, which will directly lower its temperature levels. In addition, it can be seen from Figs. 4 and 5 that, the rate of variation of the V-corrugated plate temperature along the flow direction is almost similar for all presented cases. The figures reveal that the temperature increases at a relatively high rate from the inlet edge to a distance $x/D_h = 8.4$. Then, the temperature increases at lower rate or remains almost constant up to the location at $x/D_h = 15.4$. From this location to the exit section, the plate temperature decreases monotonously for all values of Re and q_{inc} as shown in Figs. 4 and 5. The rate of decrease in the plate temperature is higher for $x/D_h = 16.7$. This can be explained as follows: from the inlet edge up to $x/D_h = 8.4$, the flow is simultaneously developing (velocity and thermal boundary layers are under development) thus the convective heat transfer coefficient is high. From the location $x/D_h = 8.4$ to 15.4 the flow is expected to become fully or nearly fully developed (thermally and hydrodynamically). Beyond $x/D_h = 15.4$ and particularly from the point $x/D_h = 16.7$ to the trailing edge, the

temperature decreases can be attributed to the adverse effect of the secondary flow in the zone behind the V-corrugated plate trailing edge up to the exit air mixer.

3.2. Effect of Reynolds number on local Nusselt number

The variation of local Nusselt number Nu_x with the axial distances x/D_h at different Re values are presented in Fig. 6 for the case of $\beta = 0°$ and different values of incident radiation heat fluxes, while, Fig. 7 shows such variations for the cases of $\beta > 0°$. Both figures show that Nu_x variations have the same trend of decreasing monotonically along the axial distances x/D_h from the inlet up to $x/D_h = 8.4$, then remains almost constant up to x/D_h around 15.4. The figures reveal that Nu_x increases as Re values increases in all cases. Such increase in Nu_x values due to increase of Re at certain axial location became more significant as β decreases and are substantial in the case of $\beta = 0°$ as shown in Fig. 6. Also, it can be seen from the figure, the effect of Re on Nu_x is more pronounced in the entrance region where the Nu_x values are higher than the rest of the channel. This is the result of simultaneously developing flow and thermal boundary layer at the channel entrance region as explained above. While, the slight increase in Nu_x values

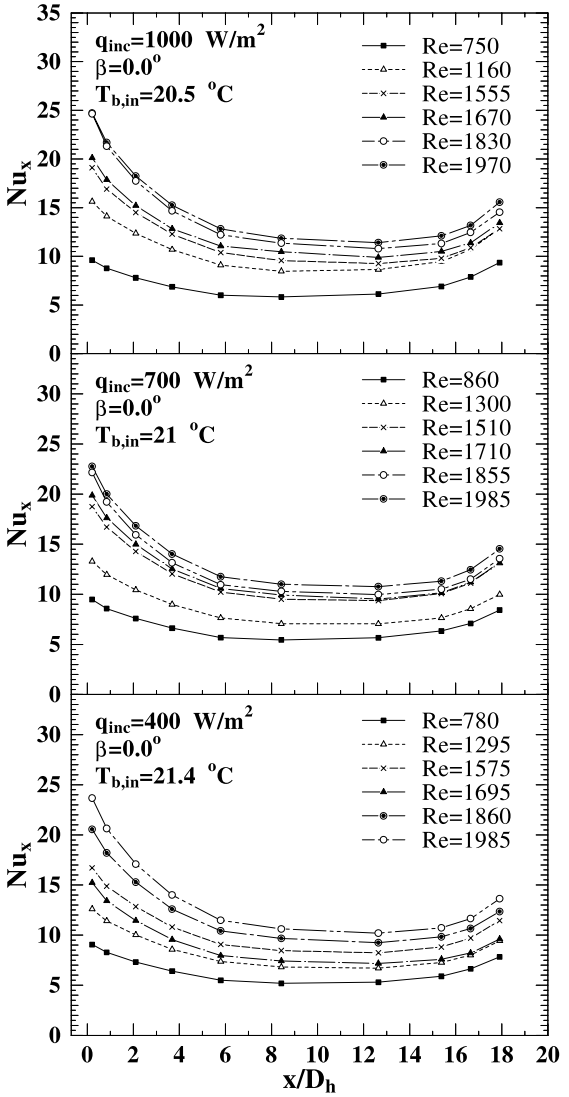

Fig. 6. Effect of Reynolds number on the local Nusselt number distributions at different incident radiation fluxes for $\beta = 0°$.

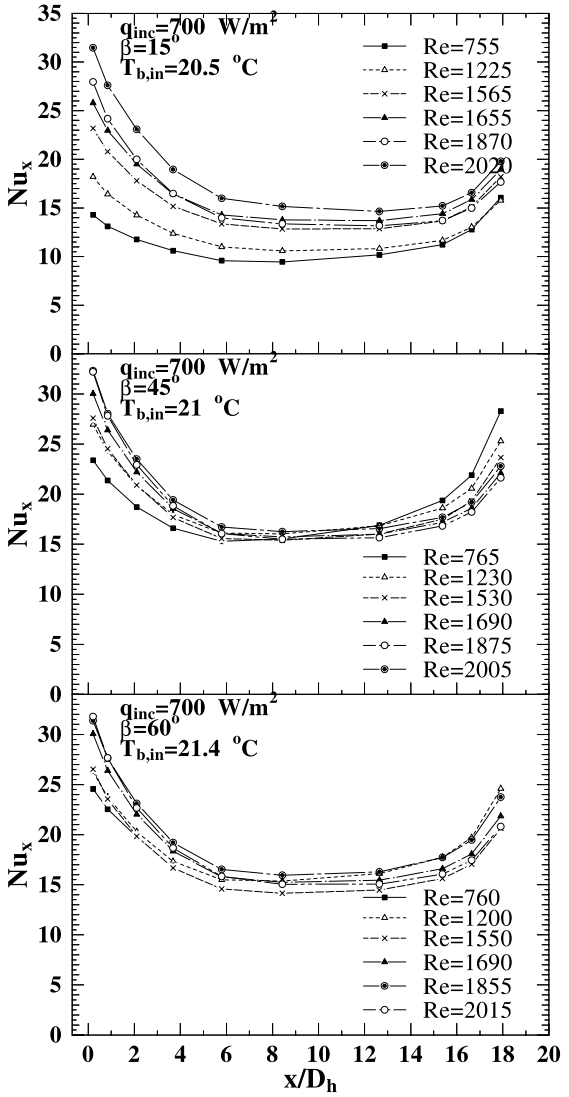

Fig. 7. Effect of Reynolds number on the local Nusselt number distributions for $\beta > 0°$ at $q_{inc} = 700$ W/m^2.

near the trailing edge of V-corrugated plate as can be seen from Figs. 6 and 7 is attributed to the effect of the secondary flow in the zone behind the trailing edge up to the exit air mixer. Such recirculating secondary flows enhance the convective heat transfer process and consequently lead to a high local convective heat transfer coefficient from the V-corrugated plate at these locations. For the cases of $\beta > 15°$ presented in Fig. 7, Nu_x variations due to changes in Re values are more pronounced at the channel entrance and exit regions than in the channel mid-section. This effect is more clear as q_{inc} increases. Explanation of the combination effect of β (buoyancy force component in the flow direction) and q_{inc} on Nu_x will be clarified in following sections.

3.3. Effect of the inclination angle on local Nusselt number

To study the effects of the buoyancy force on Nu_x, comparisons were made between runs that have same operating conditions but with different values of the inclination angle β. The results are presented in Figs. 8 and 9 for two Re values around 760 and 2020, with other operating parameters as indicated in the figures. As seen from these figures, as β increases from 0° to 60° the Nu_x values increase and effect is more significant in case of $Re = 760$. For example at $x/D_h = 8.4$ for the case of $q_{inc} = 400$ W/m^2 at $Re = 760$, Fig. 8, Nu_x value increases from 5.2 to 8.7 by a ratio of 67.3% due to changing β from 0° to 45°, while at $Re = 2050$, Fig. 9, Nu_x value

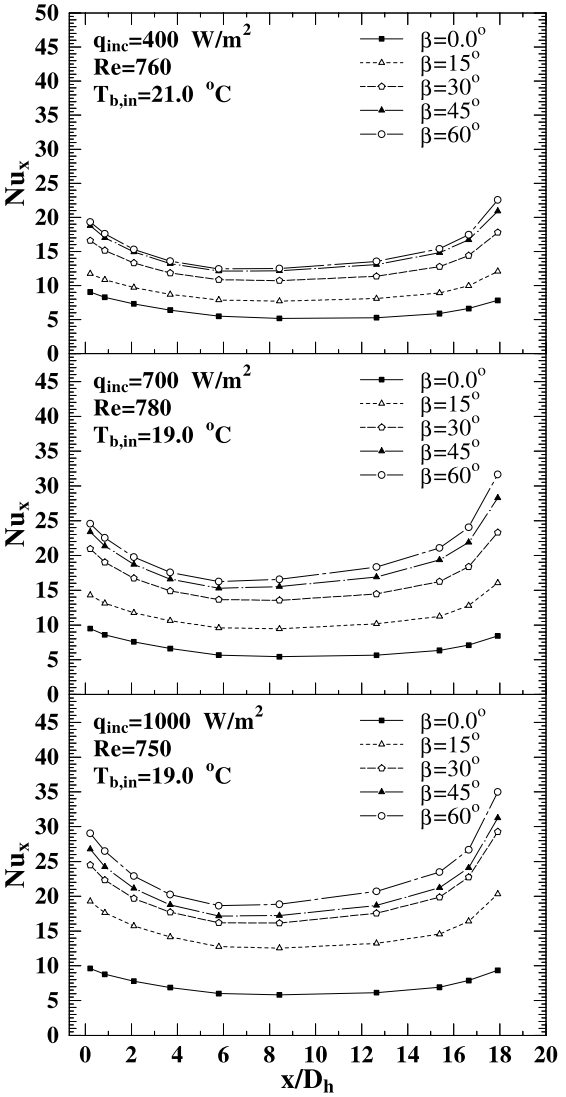

Fig. 8. Effect of the unit inclination angle (β) on the local Nusselt number for Re value around 750.

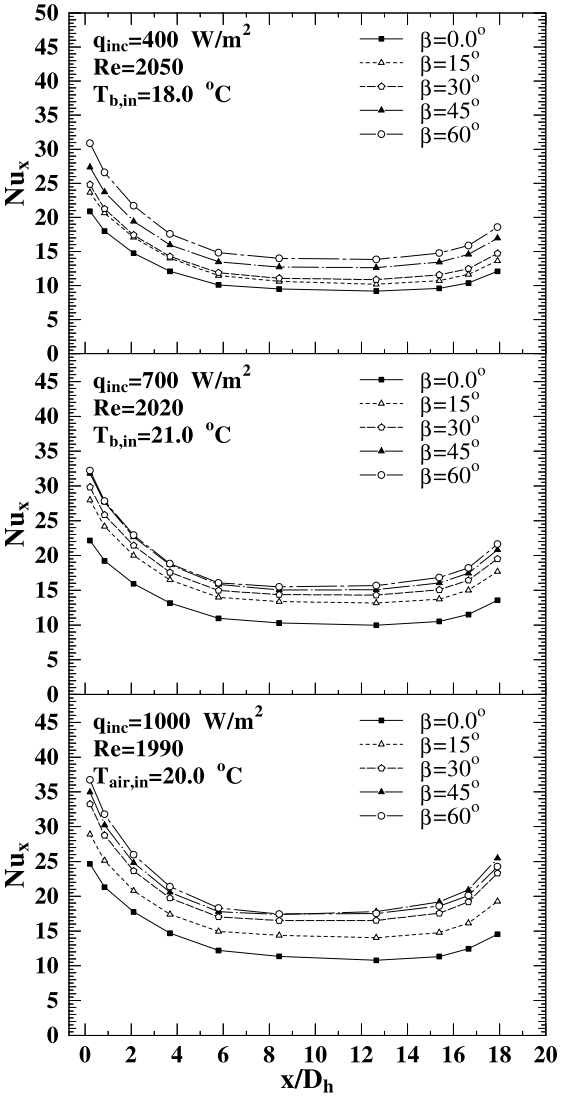

Fig. 9. Effect of the unit inclination angle (β) on the local Nusselt number for Re value around 2020.

increases from 10.6 to 14.1 by a ratio of 33% due to same change in β. These results are explained as follows: the air is flowing under the inverted heated V-shape, in case of $\beta = 0°$ the hot air stay at the apexes, however, for $\beta > 0°$, there will be buoyancy force driven the flow in the upwards direction inside the inverted V apexes (as a result of the flow direction component ($g \sin \beta$)). This leads to accelerate the fluid inside the thermal boundary layer and consequently increases the convection heat transfer rate.

3.4. Effect of incident radiation flux on local Nusselt number

The present channel configuration has thermally insulated back plate and sidewalls, while the heating source is the incident radiation flux on the V-corrugated plate. The results of experiments performed to investigate the effect of incident radiation heat flux (q_{inc}) having values of 400, 700, and 1000 W/m^2 on Nu_x are presented in Fig. 10 for Re around 760 and in Fig. 11 for $Re = 1990$. It can be seen from the figures that at all values of β, there are significant variations in Nu_x due to changes in q_{inc} values. The definition of Nu_x in this study is given by Eq. (1), in which it is based on the differences between the local V-corrugated plate temperature and local air bulk temperature ($T_{vpl,i} - T_{b,i}$). While, part of the thermal radiation heat was transferred from the V-corrugated plate ($q_{rad(bk,vpl)}$) to the flowing air by indirect method, it is absorbed in the back plate and then transferred to the flowing air by convection increasing $T_{b,i}$. As a result, the plotted Nu_x values in the figures are summation of two values that were pure convection Nusselt number plus "radiative" Nusselt number; the latter is an indirect function of the V-corrugated plate temperature, and consequently the incident radiation heat flux. The results presented in Fig. 10 for $Re = 760$

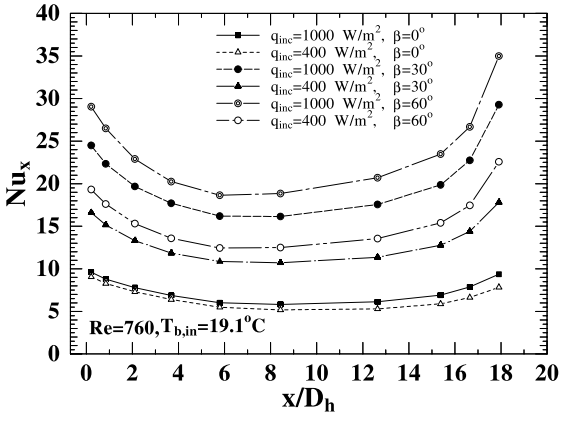

Fig. 10. Effect of the incident radiation flux (q_{inc}) on the local Nusselt number for Re value around 760.

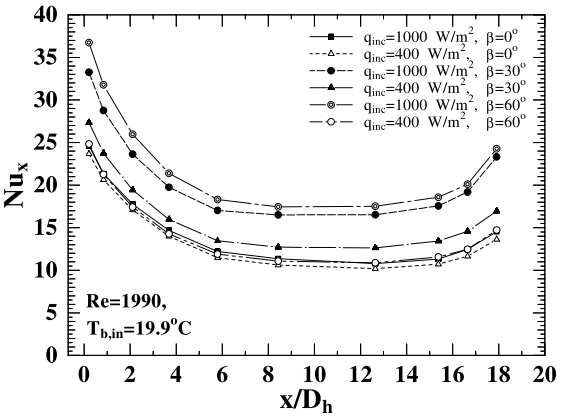

Fig. 11. Effect of the incident radiation flux (q_{inc}) on the local Nusselt number for Re value around 1990.

at $\beta = 0°$ seems to have equal values of Nu_x corresponding to the three values of q_{inc}, but quantitative numbers indicate that there are appreciable differences in the Nu_x values. At the axial distance of $x/D_h = 8.4$, measured temperature indicate that the values of ($T_{vpl,i} - T_{b,i}$) were 35.5, 55.9 and 72.3 °C corresponding to q_{inc} of 400, 700, and 1000 W/m^2 and the corresponding values of $q_{conv(vpl,air)i}$ as determined from Eq. (1) are 107.2, 183.8 and 262.3 W/m^2. Accordingly, the ratios of $q_{conv(vpl,air)i}/(T_{vpl,i} - T_{b,i})$ are 3.6, 3.2 and 3, respectively, which indicate that there is an appreciable changes in Nu_x due to changes of q_{inc} at $\beta = 0°$. In case of $\beta > 0°$, a change in q_{inc} value leads to significant increase in Nu_x value as mentioned above and shown in Figs. 10 and 11. This is due to two factors which increase the air bulk temperature and lower the V-corrugated plate temperature with the increase of q_{inc} and β. The first factor is the buoyancy driven force in the flow direction, while the second factor is the equivalent radiative convection interaction in which more thermal radiation heat is transferred from the V-corrugated plate to the back plate and convected back to the flowing air. A quantitative values for these changes are as follows: at the axial distances $x/D_h = 8.4$ of Fig. 10 and $\beta = 30°, Nu_x$ were 10.7, 13.5 and 16.1 corresponding to q_{inc} of 400, 700, and 1000 W/m^2, respectively. These results indicate that the Nu_x values increases by ratios of 26% and 50% due to changes in q_{inc} values by ratios of 75% and 150%, respectively.

3.5. Effect of inlet air bulk temperature on the local Nusselt number

It is evident for air heater solar collectors that the inlet air bulk temperature to the collector is one of the primary factors, which govern its thermal performance. It has a direct effect on decreasing both the heat removal

factor and increasing the overall heat loss coefficient. Both factors are known to be functions of the convective heat transfer coefficient between the flowing air and the hot absorber plate. To study the effect of the inlet air bulk temperature on Nu_x between the V-corrugated plate and flowing air stream, the electric heater installed before the flow fan is used to heat the inlet air stream and consequently vary its bulk temperature. The results obtained for tests performed at operating conditions of q_{inc} 1000 W/m^2, Re values of 750, 1500 and 1985 at $\beta = 45°$ and $T_{b,in}$ ranging from 12.4 to 59.4 °C, were used to estimate the variation of local Nusselt number, as shown in Fig. 12. It can be seen from this figure that there are significant increases in Nu_x values in the channel entrance region due to the increase in $T_{b,in}$ for the three Re values. The increase of the inlet air bulk temperature, increases the temperature level of the V-corrugated absorber plate. This increase in the V-corrugated plate temperature will influence the air thermal boundary layer development in the channel entrance region and consequently leads to high heat transfer rate. This influence diminishes downstream, since the heat transfer enhancement due to the simultaneous development of both the flow and thermal boundary layers also diminishes downstream.

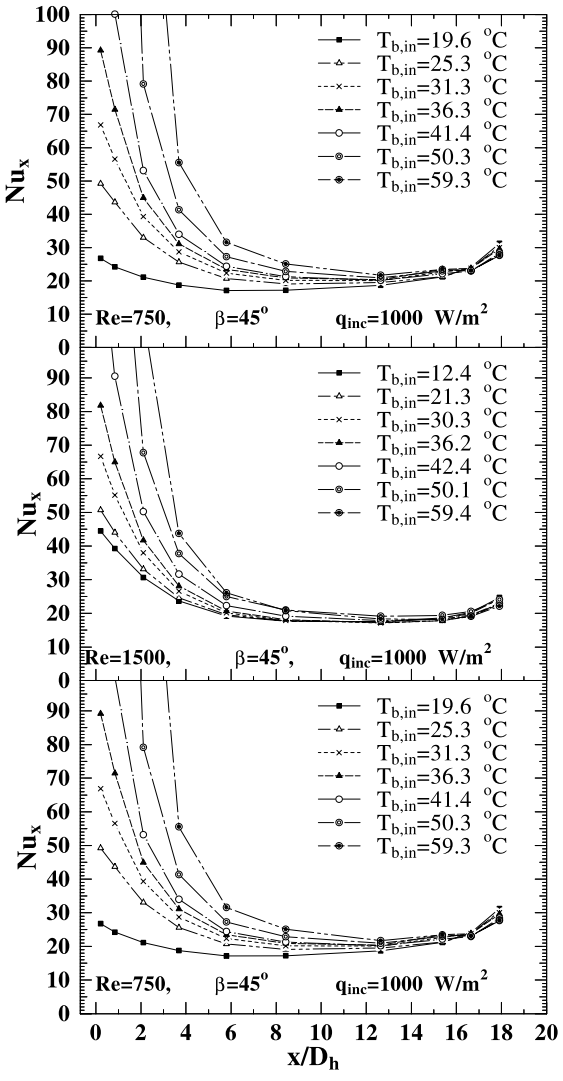

Fig. 12. Effect of inlet air bulk temperature on the local Nusselt number at different values of Re.

4. Conclusions

In this research, experimental study on effects of the operating parameters on forced-convection heat transfer for laminar flow of air in a channel having a V-corrugated upper plate heated by radiation heat flux and other walls are thermally insulated has been carried out. The parameters studied and their ranges were the flow Reynolds number (Re) ranging from 750 to 2050, incident radiation heat flux (q_{inc}) values of 400, 700, 1000 W/m^2, inlet air bulk temperature to the channel ($T_{b,in}$) changed from 12.4 to 59.4 °C and the channel inclination angle with the horizontal (β) of 0°, 15°, 30°, 45°, and 60°. The results show that:

- The effect of the flow Reynolds number values (Re) on the local Nusselt number values (Nu_x) is clear and more significant at the channel entrance region.
- Changing inclination angle with the horizontal (β) from 0° to 60° leads to an increase the local Nusselt number values (Nu_x) by a ratio ranging from 33% to 67.3% depending on Re value and other operating parameters.
- Increasing the incident radiation heat flux values (q_{inc}) by 175% and 250% leads to an increase in Nu_x values by 26% and 50%, respectively.
- The results indicate that there are significant increases in Nu_x in the channel entrance region due to the increase in inlet air bulk temperature and this influence diminishes downstream.

References

[1] E.M. Sparrow, S.H. Lin, Absorption of thermal radiation in a V-groove cavity, Int. J. Heat Mass Transfer 5 (1962) 1111–1115.

[2] R.K. Shah, A.L. London, Laminar flow forced convection in ducts, in: F. Irvine Jr., J.P. Hartnett (Eds.), Advance in Heat Transfer (Suppl. 1), Academic Press, New York, 1978, pp. 223–245.

[3] W.M. Kays, H.C. Perkins, Forced convection, internal flow in ducts, in: W.M. Rohsenow, J.P. Hartnett, E.N. Ganic (Eds.), Handbook of Heat Transfer Fundamentals, McGraw-Hill, New York, 1985, Chapter 7.

[4] R.K. Shah, M.S. Bhatti, Laminar convective heat transfer in ducts, in: S. Kakac, R.K. Shah, W. Aung (Eds.), Handbook of Single-Phase Convective Heat Transfer, Wiley/Interscience, New York, 1987, Chapter 3.
[5] Y. Piao, E.G. Hauptmann, M. Iqbal, Forced connective heat transfer in cross-corrugated solar air heaters, J. Solar Energy Eng. 116 (1994) 212–214.
[6] C.H. Liu, E.M. Sparrow, Convective-radiation interaction in a parallel plate channel-application to air-operated solar collectors, Int. J. Heat Mass Transfer 23 (1980) 1137–1146.
[7] I. Satoh, Y. Kurosaki, Heat transfer combined with convection and radiation in an asymmetrically heated duct, in: Proceedings of ASME-JSMME Thermal Engineering Joint Conference, Honolulu, Hawaii, vol. 5, March 22–27, 1987, pp. 325–332.
[8] Ahmed Hamza H. Ali, Study on characteristics and design parameters of laminar flow forced-convection heat transfer in channel with offset plates heated by radiation, Ph.D. Thesis, Muroran Institute of Technology, Hokkaido, Japan, 1998.
[9] JIS A 4112-1994, Japanese industrial standard solar collectors, revised 1994-20-01, Japanese Standards Association, Japan, 1994.
[10] BSI-BS6757: 1986, British standard methods of test for thermal performance of solar collectors, British Standard Institution, London, 1986.
[11] S.M. El-Sherbiney, K.G.T. Hollands, G.D. Raithby, Free convection across inclined air layers with one surface V-corrugated, J. Solar Energy Eng. 100 (1978) 410–415.
[12] T. Fujii, H. Imura, Natural convection heat transfer from a plate with arbitrary inclination, Int. J. Heat Mass Transfer 15 (1972) 755–767.
[13] J.P. Holman, Experimental Methods for Engineering, second ed., McGraw-Hill Kogakusha, Tokyo, 1971.
[14] E.O. Doblen, Measurement Systems Application and Design, McGraw-Hill, New York, 1990.